RSC Advances

PAPER

View Article Online
View Journal | View Issue

Cite this: *RSC Adv.*, 2024, **14**, 16284

Highly sensitive sensing of CO and HF gases by monolayer CuCl

Shamiala Pervaiz,[a] M. Usman Saeed,[a] Sehrish Khan,[a] Bisma Asghar,[a] Y. Saeed, *[a] Hosam O. Elansary[bc] and A. U. R. Bacha [d]

Using a first-principles approach, the adsorption characteristics of CO and HF on a CuCl monolayer (ML) are studied with Grimme-scheme DFT-D2 for accurate description of the long-range (van der Waals) interactions. According to our study, CO gas molecules undergo chemisorption and HF gas molecules show a physisorption phenomenon on the CuCl monolayer. The adsorption energy for CO is −1.80 eV, which is quite a large negative value compared to that on other previously studied substrates, like InN (−0.223 eV), phosphorene (0.325 eV), Janus Te_2Se (−0.171 eV), graphene (P-graphene, −0.12 eV, B-graphene, −0.14 eV, N-graphene, −0.1 eV) and monolayer ZnS (−0.96 eV), as well as pristine hBN (0.21 eV) and Ti-doped hBN (1.66 eV). Meanwhile, for HF, the adsorption energy value is −0.31 eV (greater than that of Ti-doped hBN, 0.27 eV). For CO, the large value of the diffusion energy barrier (DEB = 1.26 eV) during its movement between two optimal sites indicates that clustering can be prevented if many molecules of CO are adsorbed on the CuCl ML. For HF, the value of the DEB (0.082 eV) implies that the adsorption phenomenon may happen quite easily upon the CuCl ML. The transfer of charge according to Bader charge analysis and the variation in the work function depend only on the properties of the elements involved, *i.e.*, their nature, rather than the local binding environment. The work function and band-gap energy variation of the CuCl ML (before and after adsorption) show high sensitivity and selectivity of CO and HF binding with the CuCl monolayer. HF molecules give a more rapid recovery time of 1.09×10^{-7} s compared to that of CO molecules at a room temperature (RT) of 300 K, which indicates that the necessary adsorption and reusability of the CuCl ML for HF can be accomplished effectively at RT. Significant changes in the conductivity are observed due to the CO adsorption at various temperatures, as compared to adsorption of HF, which suggests the possibility of a modification in the conductivity of the CuCl ML.

Received 27th February 2024
Accepted 4th May 2024

DOI: 10.1039/d4ra01519c

rsc.li/rsc-advances

1. Introduction

Quality and quantity control of air and toxic gases, respectively, and their monitoring in outdoor as well as indoor environments, like factories, workplaces, laboratories and various industrial settings, have become a serious matter of concern as a result of large emissions of harmful and toxic gases. CO and HF are present in the atmosphere as colorless gases and are produced by partial combustion of organic molecules and in industrial chemical plants, respectively. Continuous and long exposure to these toxic gases can cause serious environmental and health issues.[1,2] Their exposure can result in strong irritation in the respiratory tract, eye redness, gastrointestinal diseases, rhinorrhea, neurological effects, cough, headache, dermatalgia and other symptoms. Any leakage of these hazardous gases can cause explosions, leading to various kinds of destruction. So, a great deal of work has been carried out for the precise analysis of these gases.[3]

Gas sensors are devices using gas sensing materials for the determination of the concentration and composition of gases in the surrounding area. Therefore, gas sensors are not only used in industry, but also in the field of biomedicine, where they are utilized to investigate exhaled gases to identify different kinds of illness.[4] Therefore, gas sensing technology needs to show high performance as demanded for national safety and by different industries.[5] In the gas-detection mechanism, the adsorbed gas molecules can donate or accept electrons from the substrate, resulting in a variation in electrical resistance. So, in this way the presence of gas molecules is detected by the gas

[a]*Department of Physics, Abbottabad University of Science and Technology, Abbottabad, KPK, Pakistan. E-mail: yasir.saeed@kaust.edu.sa; yasirsaeedphy@aust.edu.pk; Tel: +(92)-3454041865*

[b]*Prince Sultan Bin Abdulaziz International Prize for Water Chair, Prince Sultan Institute for Environmental, Water and Desert Research, King Saud University, Riyadh 11451, Saudi Arabia*

[c]*Department of Plant Production, College of Food & Agriculture Sciences, King Saud University, Riyadh 11451, Saudi Arabia*

[d]*State Key Laboratory of Urban Water Resource and Environment, Shenzhen Key Laboratory of Organic Pollution Prevention and Control, School of Civil and Environmental Engineering, Harbin Institute of Technology Shenzhen, Shenzhen 518055, P. R. China*

sensor. Usually, there are some basic criteria and performance parameters for gas sensors: (a) high sensitivity; (b) high selectivity; (c) stability in performance; (d) fast response; (e) low working temperature and (f) low power consumption. Conventional semiconductor gas sensing technologies, using SnO_2, TiO_2, ZnO, and Cu_2O (semiconducting thin films), are widely studied and employed practically.[6–8] However, such gas sensors consisting of metal oxides need high temperatures for their operation, some working at temperatures higher than 150 °C, to enhance the chemical reactivity of the gas with the sensing material. As a result of this, the energy consumption increases, therefore reducing their suitability under daily environmental conditions. Room temperature (RT) sensors are lower-cost because they do not need heat for their operation.

Recently, with the progress in low-dimensional semiconductors, 2D materials have attracted much consideration. By using 2D materials, low-power and high-density gas sensors with more sensitivity can be developed. The large surface–volume ratio of 2D materials enables them to have high sensitivity and greater recovery efficiency.[9,10] They have good conducting and semiconducting features. Surface modifications can also be carried out on these materials due to weak van der Waals forces, which make 2D materials more suitable when compared with 0D and 1D materials. 2D materials can be categorized as: (a) the graphene family;[11] (b) 2D metal oxides;[12] (c) transition metal dichalcogenides (TMDCs)[13] like WS_2,[14] WSe_2,[15] MoS_2,[16,17] and so on; (d) MXenes;[18] and (5) materials based on a single element, like black phosphorous,[19] arsenene,[20] and antimonene.[21]

Cuprous chloride (CuCl) is an ionic semiconductor that has various different applications. It is an essential chemical product in fields like metallurgy, pigments, petrochemicals, and medicine. It is in the class of binary compounds that are tetrahedrally coordinated. These compounds hold huge interest for the research field as well as for understanding basic semiconductor physics. CuCl is a semiconductor with a large band gap[22] and is studied for its linear and non-linear optical properties.[23] The fundamental electronic structure of CuCl has been studied by various groups using density functional theory (DFT).[24,25] CuCl has amazing tunable properties in nanoelectronics, including for gas sensing.[26–29] CuCl monolayers, having a two-dimensional structure, possess promising properties in gas sensing owing to their high surface–volume ratio. Sun *et al.*,[30] Kou *et al.*,[31] Zhu *et al.*,[32] and Zhang *et al.*[33] have studied CO adsorption on InN, phosphorene, Janus Te_2Se and doped graphene monolayers. Recent studies also demonstrated HF and CO adsorption.[34,35] N. Ahmadian *et al.* discovered an appropriate and sensitive sensor for dimethyl methylphosphonate (DMMP, a nerve agent) on the exterior surface of defect-containing semiconducting (10,0) single-wall carbon nanotubes (SWCNTs), by using first-principles van der Waals density functional (vdW-DF) calculations.[36] M. D. Ganji *et al.* studied the adsorption of formaldehyde (H_2CO) on graphene, hexagonal silicon carbide (h-SiC) and hexagonal aluminum nitride (h-AlN) monolayer sheets for application as gas sensors.[37] M. D. Ganji *et al.* also used DFT simulations to study the adsorption characteristics of acetone on zigzag single-walled boron nitride nanotubes (BNNTs).[38] T. Banibairami *et al.* used vdW-DF to assess the adsorption of the gas molecule phosgene ($COCl_2$) on a hexagonal aluminum nitride (h-AlN) nanosheet.[39] Here, in our theoretical research, the gas sensing properties of CuCl MLs for CO and HF are studied in detail, which has not been presented before.

Using a first-principles study based on DFT, the adsorption of CO and HF gaseous molecules on CuCl MLs is studied. Correction in the van der Waals interactions is carried out *via* DFT-D2 and the Hubbard potential (U) is introduced to take into account the electronic interactions for the strongly correlated orbitals. Geometry optimization is carried out to get highly stable configurations.

2. Computational detail

For the structural optimization and investigation of electronic properties, an *ab initio* code, namely the Quantum Espresso (QE) package,[40] is used. The generalized gradient approximation (GGA) in the Perdew–Burke–Ernzerhof (PBE) functional[41] is employed for the plane-wave basis set in order to relax the structures, and ultra-soft pseudo-potentials[42] were adopted for expressing valence electrons and ionic core interactions. In addition, Grimme-scheme DFT-D2 was utilized[43] for accurate description of the long-range (van der Waals) interactions between the monolayer and gas molecules. The DFT+U method is used for considering the Coulomb repulsion interaction of electrons in the Cu:3d and Cl:3p orbitals, and it is also used for the correction of the self-interaction error (SIE), which is involved in the s, p, d and f states.[44] So, for this purpose, the addition of the Hubbard parameter (U), is carried out in the PBE functional.[45,46] The U parameters were adopted according to Monteiro *et al.*[47] as U (Cu:3d) = 7.0 eV and U (Cl:3p) = 7.0 eV, which are attained using the ACBN0 method.[48]

A CuCl monolayer with a 3 × 3 supercell is used, comprising 18 atoms of Cu and Cl (nine for each). To keep apart the adjacent periodic images of the 2D layer of the simulated supercell geometry, a vacuum of 20 Å is set. Structural relaxation is carried out unless the force on an individual atom is less than 0.005 eV $Å^{-1}$. A kinetic-energy cutoff for the wave function of 650 eV and an energy convergence value of 10^{-8} eV is used. TheMonkhorst–Pack scheme[49] is used for first Brillouin-zone representation with a 4 × 4 × 1 k-mesh. For the accuracy of the electronic calculations, a dense k-mesh of 12 × 12 × 1 is used for Brillouin-zone sampling. Bader charge analysis[50] is employed to investigate the charge that is transferred between the CuCl ML and gas molecule. To evaluate the strength of the adsorption phenomenon of the gas molecule on the CuCl ML, the following relation is used:

$$E_{ads} = E_{total} - (E_{CuCl} + E_{gas\ molecule}) \quad (1)$$

where E_{ads} is the adsorption energy, E_{total} is the total energy of the combined system (a gas molecule adsorbed on the CuCl ML), E_{CuCl} is the energy of the pristine CuCl ML and $E_{gas\ molecule}$ is the energy of the gas molecule.

In order to locate the lowest energy pathway between the initial and final coordinates during the adsorption phenomenon, the climbing image nudged elastic band (CI-NEB) method is adopted. For this purpose, a transition state search (TSS) is carried out. The diffusion energy barrier (DEB) is calculated as:

$$E_{\mathrm{DEB}} = E_{\mathrm{TS}} - E_{\mathrm{IS}} \quad (2)$$

where E_{TS} is the transition-state energy and E_{IS} is the initial-state energy.

The conductivity of the CuCl ML also varies due to the adsorption phenomenon of the gaseous molecules, which is determined by the equation given below.

$$\sigma = \exp\frac{-E_g}{2kT} \quad (3)$$

where σ denotes the electrical conductivity, T is the temperature, E_g represents the band-gap energy and k denotes the Boltzmann constant.

For the determination of the recovery time of the gaseous molecules, the following relation is used:

$$\tau = {\nu_0}^{-1} \mathrm{e}^{\frac{-E_{\mathrm{ads}}}{kT}} \quad (4)$$

where E_{ads} is the adsorption energy, ν_0 ($=10^{12}$ s^{-1})[51] is the attempt frequency, T is the temperature and k ($=8.617 \times 10^{-5}$ eV K^{-1}) is the Boltzmann constant.

The work function is the least amount of energy needed for electron ejection from the Fermi level to infinity, for the adsorbed gas molecules. The work function is calculated using the following equation:

$$\phi = V(\phi) - E_{\mathrm{Fermi}} \quad (5)$$

where ϕ denotes the work function, $V(\phi)$ is the electrostatic potential and E_{Fermi} is the Fermi energy of the CuCl ML.

3. Results and discussion

For the optimized binding configuration, four adsorption sites on the relaxed pristine CuCl ML are considered for the adsorption of CO and HF. Sites 1 and 2 represent the tops of the Cu atom and Cl atom, respectively. The top of the Cu–Cl bond is site 3 and site 4 represents the CuCl hexagon center, as shown in Fig. 1.

The dynamic stability of the CuCl ML structure has been assessed by observing the lattice vibrations with the phonon dispersion plot, as shown in Fig. 2. Only one mode of the phonon dispersion plot of the CuCl ML exhibits a slight imaginary frequency, in the range of about 11 cm^{-1} within the $M \rightarrow \Gamma$ high symmetry k-point path, in accordance with a previous theoretical study on the CuCl ML.[27] This further suggests that it can be stabilized on supporting materials because suitable substrates have always been used in the synthesis of such monolayer-based structures.[52] As an example, the synthesis of a thin layer of copper iodide is carried out on top of a Cu (111) surface.[53] Moreover, an ionic magnesium chloride monolayer structure has been produced on Pd, Pt, and Rh metal surfaces.[54] As a result, we anticipate that such an ML structure may also be achievable through experimentation.

The adsorption energy of CO and HF on the CuCl ML is calculated by using eqn (1). According to our calculations, site 1 (Cu atom top) gives the maximum value of adsorption energy for CO, and for HF, site 2 (Cl atom top) is the maximum adsorption energy site. Each gaseous molecule is diatomic, so all the feasible orientations are considered, *i.e.*, they have two possible orientations at the respective sites of maximum adsorption energy, with either of the atoms in the gaseous molecule pointing towards Cu or Cl. The proposed sites result in the configurations shown in Fig. 3, after many minimization steps in each optimization.

The absorption sites with their energies for CO and HF molecules are given in Table 1. It is observed that the adsorption results in the structural deformation of the CuCl ML (Fig. 3). Both the molecules show a vertical alignment with respect to the CuCl ML. In the case of CO, the C atom points towards Cu atom (Fig. 3a). For the HF molecule, the H atom points towards Cl atom (Fig. 3b). It is found that CO gas molecules show chemical adsorption to the CuCl ML, with an adsorption energy value of −1.80 eV. So, it is concluded that the CuCl ML shows a very good adsorption performance for CO gas molecules in comparison with that of other substrates in previous studies, like InN (−0.223 eV), phosphorene (0.325 eV),

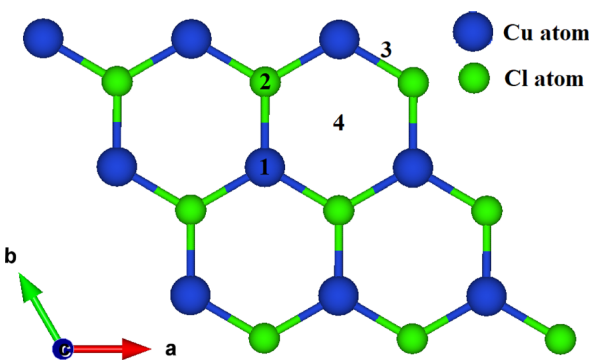

Fig. 1 CuCl ML, with different adsorption sites.

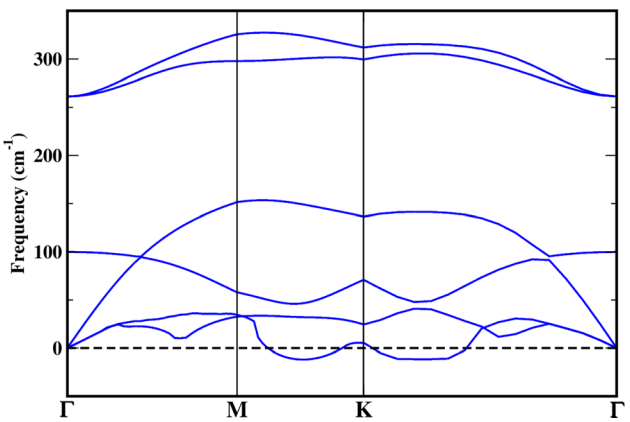

Fig. 2 Phonon dispersion of the CuCl monolayer.

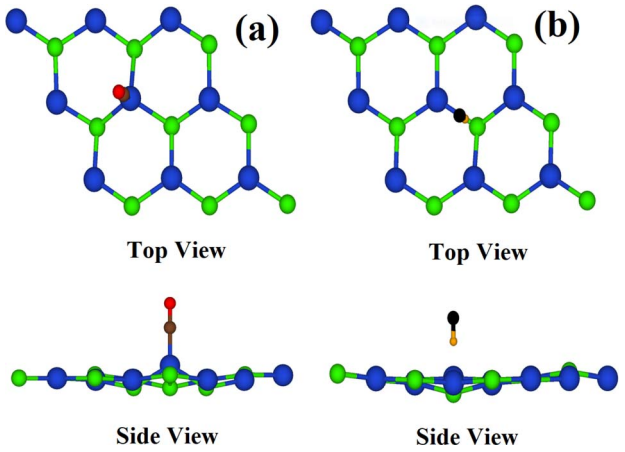

Fig. 3 Top and side views of the optimized configurations for adsorption of (a) CO and (b) HF on the CuCl ML. (Colour code: brown, carbon; red, oxygen; yellow, hydrogen; black, fluorine).

Table 1 Adsorption energies (E_{ads} (eV)), minimum adsorption heights (h), charge transfers (Q), and diffusion energy barriers (DEBs) for the CuCl ML

Molecule	Site	h (Å)	E_{ads} (eV)	Q (e)	DEB
CO	Cu (site 1)	1.79	−1.80	0.03	1.26
	Cl (site 2)	3.35	−0.12	0.02	—
	Bridge (site 3)	1.74	−1.78	0.01	—
	Centre (site 4)	2.37	−0.30	0.01	—
HF	Cu (site 1)	2.21	−0.22	−0.03	—
	Cl (site 2)	2.09	−0.31	−0.04	0.08
	Bridge (site 3)	2.10	−0.28	−0.021	—
	Centre (site 4)	1.60	−0.26	−0.02	—

Janus Te_2Se (−0.171 eV), graphene (P-graphene, −0.12 eV; B-graphene, −0.14 eV; N-graphene, −0.1 eV), and monolayer ZnS (−0.96 eV), as well as pristine hBN (0.21 eV) and Ti-doped hBN (1.66 eV).[30–35] Meanwhile, the HF molecule shows physical adsorption to the CuCl ML, with a smaller physical adsorption energy of −0.31 eV. Even so, the CuCl monolayer shows a better adsorption energy for HF molecules as compared to that of Ti-doped hBN, 0.27 eV.[35] The adsorption of CO and HF molecules is exothermic, as indicated by the negative values of the adsorption energy. Optimal distances of 1.79 Å and 2.09 Å from the CuCl ML are observed for the CO and HF gas molecules, respectively.

The transition-state search is carried out for more understanding of the optimized configuration of CO and HF. For this purpose, two adsorption sites are selected, as shown in Fig. 4. The nudged elastic band (NEB) model is used to obtain the minimum energy path between the reactants and products. The paths with their energies indicate that for the adsorption of CO and HF, the lowest-energy site is chosen, which provides proof that the calculated adsorption energy is accurate. Two adsorption states, TS1 and TS2, are noticed in the case of the CO-CuCl system, and for the calculation of the diffusion energy barrier (DEB), transition state TS2 is considered. An intermediate state

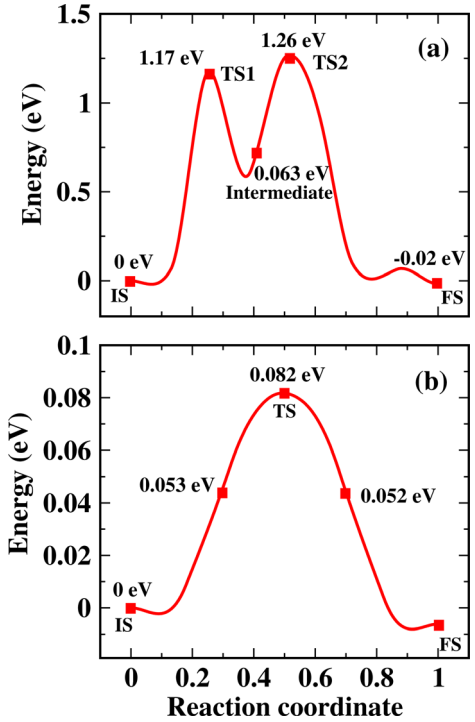

Fig. 4 Diffusion energy barriers and diffusion pathways of (a) CO and (b) HF. IS is the initial state, FS is the final state and TS is a transition state.

is also observed in this case, which is a short-lived and unstable state during the adsorption of the gas molecule, between the initial site and final optimal state. Here, in the case of CO-CuCl, the gas molecule CO is briefly adsorbed by the Cl atom on the way from TS1 to TS2. By using eqn (2), the DEB is calculated. The values of the DEB for CO and HF on the surface of the CuCl ML are found to be 1.26 eV and 0.08 eV, respectively. In the case of CO, the greater DEB value indicates that clustering may be avoided when many molecules of CO are introduced on the CuCl ML. However, it is concluded that the binding phenomenon may occur more easily in case of HF upon the CuCl ML, as suggested by its DEB value, even in the absence of external energy.

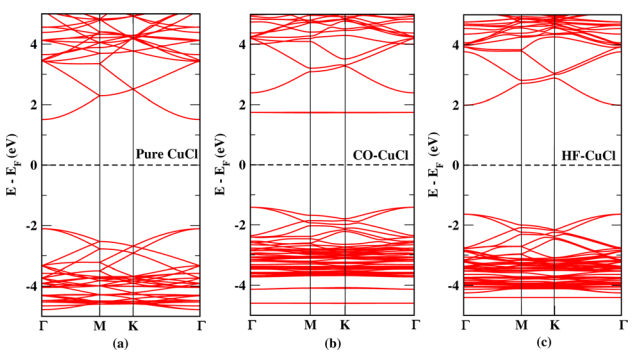

Fig. 5 Band structures of (a) the CuCl ML, (b) CO adsorbed on CuCl and (c) HF adsorbed on CuCl.

The calculation of electronic properties is carried out for understanding the interaction of the CuCl ML with the gas molecules. Fig. 5a shows the band structure for the pristine CuCl ML with a band gap of 3.66 eV, which is in accordance with that from previous DFT studies (3.66 eV) and much greater than the 1.1 eV obtained with GGA-PBE.[27] Both the adsorbed systems, CO and HF on the CuCl ML, show a small increase in the number of conduction bands as compared to the pristine CuCl system (Fig. 5(b) and (c)).

It is also observed that the band-gap energy decreased to 3.14 eV in the case of the CO-CuCl system and 3.56 eV for the HF-CuCl system, as given in Table 2.

According to our calculations, the CuCl ML has a nonmagnetic nature with and without the adsorption of CO and HF. To analyze the contribution of the CO and HF adsorbed on the CuCl ML and the newly appearing band lines, the total density of states (TDOS) and projected density of states (PDOS) are plotted (Fig. 7a and b) in comparison to those of the pristine CuCl ML (Fig. 6). New peaks are observed at about 1.75 eV (due to C 2p and O 2p orbitals) in case of CO-CuCl, whereas a peak is observed at about −4.4 eV (due to F 2p orbitals) for the HF-CuCl system. Moreover, the three systems, *i.e.*, pristine CuCl, CO-CuCl and HF-CuCl, have filled valence bands due to the bonding states (Cu d and Cl p orbitals). In contrast, the conduction-band bottom is made from the unoccupied orbitals (Cu s, d and Cl p) for the pristine CuCl system.

Bader charge analysis gives the charge transfer between the CuCl monolayer and gaseous molecules. It is calculated that the charge transfer between the HF and CuCl monolayer is $-0.04e$, which is a bit greater than that in previous studies,[35] and similarly we observed a high charge transfer of $0.03e$ for the CO/CuCl ML as compared to that in previous studies.[30,32–35] It is observed from the calculations that the charge transfer is independent of the Hubbard parameter, *i.e.*, the local binding environments, and only relies upon the properties of the adsorbed gas and the nature of the monolayer, which is compatible with the findings of previous studies.[55]

Furthermore, the calculation of electronic charge density difference is carried out to provide more insight into the charge transfer for the CO-CuCl and HF-CuCl systems, as displayed in Fig. 8a and b, respectively. The cyan colour shows charge depletion, whereas the yellow colour shows charge accumulation at an isovalue of 0.97 meV A^{-3}. The CO gas molecule behaves as a charge donor due to charge accumulation on the CuCl ML, whereas HF accepts electrons from CuCl and behaves as a charge acceptor. These results are in accordance with the Bader charge analysis. The shifting of charge due to exposure to gases has a major influence on the resistance. The reduction of charge carriers takes place due to charge depletion in the monolayer and increases its resistance. However, reduction in the resistance takes place as a result of accumulation of charges in the monolayer, because accumulation increases the charge carriers.

Table 2 Band-gap energies (E_g) and work functions (ϕ) of CuCl and with gas-molecule adsorption

System	E_g (eV)	ϕ (eV)
CuCl ML	3.66	4.26
CO-CuCl	3.14	4.48
HF-CuCl	3.56	4.74

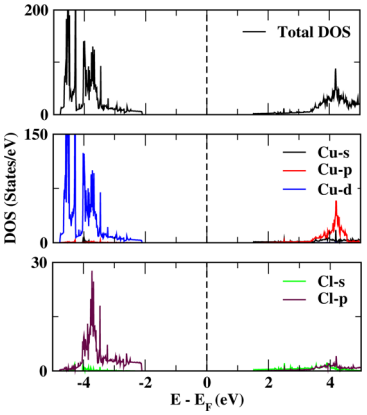

Fig. 6 Projected density of states (PDOS) of the pristine CuCl.

Determination of the recovery time is required to find the reusability of the gas sensors. It is calculated for CO and HF at various temperatures using eqn (4). Fig. 9 shows the plot of the recovery time. It is observed that at RT, the value of the recovery time of CO on CuCl ML is 1.69×10^{18} s, while HF molecules show a more rapid recovery time of 1.09×10^{-7} s, which is much less than that found in previous studies on HF (4.68 min).[34] This indicates that we can achieve active sensing with a fast recovery time for HF at RT (300 K).[56,57] Further calculations are carried out to determine the changes with various temperatures. At 200 K, CO gave a recovery time of 1.5×10^{33} s and for HF its value is 4.4×10^{-5} s. Moreover, at a high temperature of 400 K, the recovery time of CO is 4.70×10^{10} s and for HF its value is 6.0×10^{-9} s, as shown in Fig. 9. Lowering the

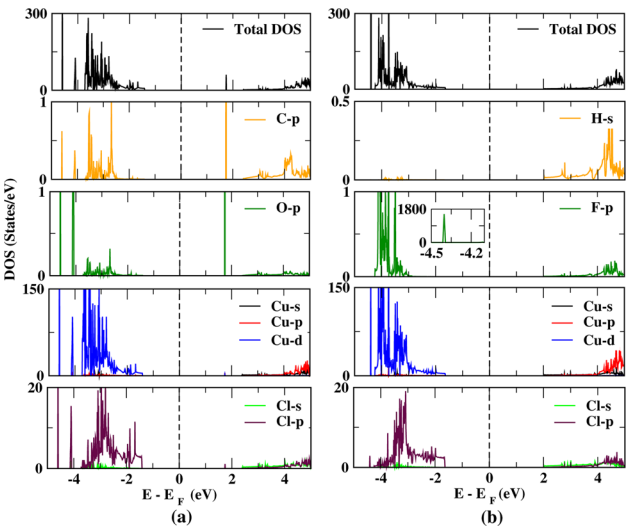

Fig. 7 Projected density of states (PDOS) the (a) CO-CuCl and (b) HF-CuCl systems.

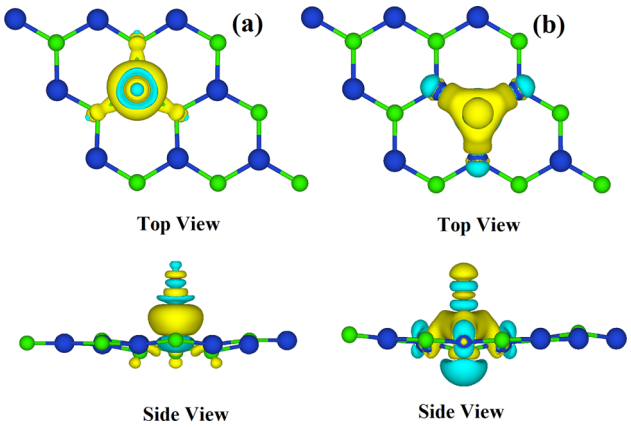

Fig. 8 Charge density difference of (a) CO-CuCl and (b) HF-CuCl.

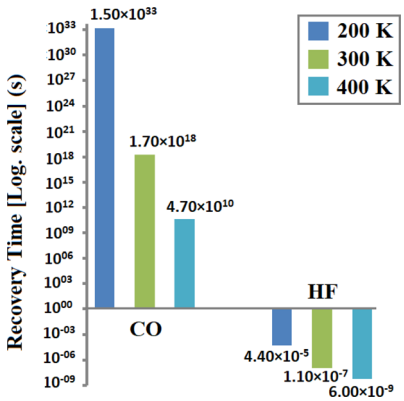

Fig. 9 Recovery times for CO and HF adsorbed on the CuCl monolayer.

temperature gives a higher recovery time, whereas an elevation in the temperature reduces its value to an acceptable range. For CO molecules, the recovery time can be reduced by increasing the temperature or by using UV radiation (attempt frequency $\nu_0 = 10^{15}\ s^{-1}$). This observation suggests that the reusability and required sensing of HF on the CuCl ML may be achieved efficiently at RT.

Moreover, the variation in the carrier mobility also brings changes in the conductivity of the CuCl ML due to gas adsorption, which is determined using eqn (3). The conductivity shows a direct relation to the exponential of band gap. Any variation in the band-gap width alters the conductivity. Our calculations show a band-gap energy difference of 0.52 eV for CO adsorption and 0.1 eV for HF adsorption on the CuCl ML. The energy change in the gap before and after adsorption shows high selectivity for CO and HF with the CuCl monolayer. Although there is less observed band-gap energy variation, its exponential value leads to a notable change in the conductivity at various temperatures. This observation shows the possibility of a modification in the conductivity of the CuCl ML due to CO and HF adsorption. This also suggest that CO and HF can be distinguished through the energy-gap variation measurement.

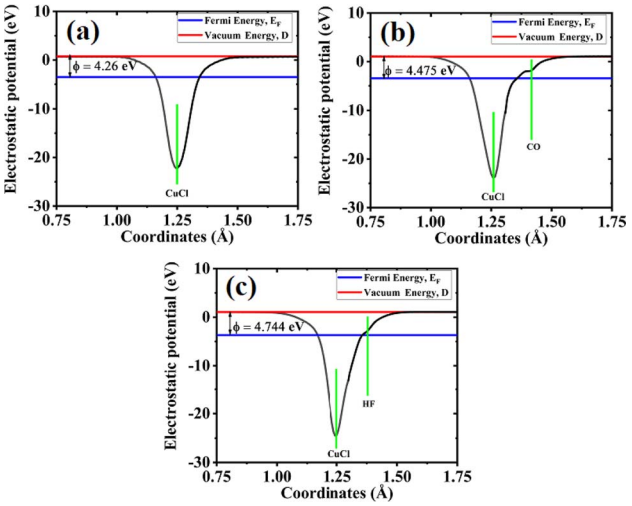

Fig. 10 Work functions for the (a) CuCl ML, (b) CO-CuCl and (c) HF-CuCl systems.

The work function is the difference between the electrostatic potential in a vacuum and the Fermi level. It is calculated using eqn (5). The work function for the pristine CuCl ML is 4.26 eV, whereas after the adsorption of gas molecules on the CuCl ML, the value of the work function is increased to 4.475 eV for CO molecules and 4.74 eV for HF, as shown in Fig. 10a–c. The work function is related to the conductivity, because it changes due to variations in the charge concentration.[58] Similar to the Bader charge analysis discussed earlier, the local binding environment also does not affect the work-function variation, but its dependence is on the nature of the elements involved. On the whole, the work-function variation confirms a strong interaction of CO and HF with the CuCl ML, which indicates the sensitivity of the CuCl ML to CO and HF molecules.

4. Conclusion

Our DFT+U study suggests that the CuCl monolayer shows favorable chemical adsorption for the CO molecule and physical adsorption for the HF gas molecule. CO possesses a quite strong adsorption energy of −1.80 eV, whereas HF has a −0.31 eV adsorption energy. For the CO gas molecule, the large value of the diffusion energy barrier (DEB) during its movement between two optimal sites indicates that clustering can be prevented if many molecules of CO are adsorbed on the CuCl ML. For HF, the value of the DEB implies that the adsorption phenomenon may happen quite easily upon the CuCl ML. The transfer of charge according to the Bader charge analysis and the variation in the work function depend only on the properties of the elements involved, *i.e.*, its nature, rather than the local binding environment. The difference in the work function of the CuCl ML (before and after adsorption) verifies the presence of a strong interaction and the high sensitivity of the CuCl monolayer to CO and HF gas molecules. This change also suggests that both gases, CO and HF, can be distinguished through the work-function measurement. HF molecules show

a more rapid recovery time than CO molecules at room temperature, which indicates that the necessary adsorption and reusability of CuCl ML for HF can be accomplished effectively at 300 K. Significant changes in the conductivity are observed due to the CO adsorption at various temperatures as compared to HF, suggesting the possibility of a modification in the conductivity of the CuCl ML and showing high selectivity of the CuCl ML for CO and HF. These findings show that the CuCl monolayer could be a promising candidate for CO and HF adsorption. This research study is expected to give a better insight into the sensing properties of the CuCl ML and the chances of tuning such properties by effective means in future studies.

Conflicts of interest

The authors declare that they have no known competing financial interests or personal relationships that could have appeared to influence the work reported in this paper.

Acknowledgements

The authors extend their appreciation to the Deanship of Scientific Research, King Saud University for funding through the Vice Deanship of Scientific Research Chairs; Research Chair of Prince Sultan Bin Abdulaziz International Prize for Water. The author Y. Saeed would like to thank the Higher Education Commission (HEC) of Pakistan for providing a grant under NRPU-15844.

Notes and references

1 S. Y. Cho, K. H. Woo, J. S. Kim, S. Y. Yoon, J. Y. Na, H. H. Yu and Y. B. Kim, Acute Symptoms in Firefighters who Participated in Collection Work after the Community Hydrogen Fluoride Spill Accident, *Ann. Occup. Environ. Med.*, 2013, **25**, 36–41.

2 H. D. Kuhns, C. Mazzoleni, H. Moosmüller, D. Nikolic, R. E. Keislar, P. W. Barber, Z. Li, V. Etyemezian and J. G. Watson, Remote sensing of PM, NO, CO and HC emission factors for on-road gasoline and diesel engine vehicles in Las Vegas Nevada, *Sci. Total Environ.*, 2004, **322**, 123–137.

3 S. Zhang, J. Guo, L. Liu, H. Ruan, C. Kong, X. Yuan, B. Zhang, G. Gu, P. Cui, G. Cheng and Z. Du, The self-powered artificial synapse mechanotactile sensing system by integrating triboelectric plasma and gas-ionic-gated graphene transistor, *Nano Energy*, 2022, **91**, 106660–106668.

4 N. Nasiri and C. Clarke, Nanostructured gas sensors for medical and health applications: Low to high dimensional materials, *Biosensors*, 2019, **9**, 43–64.

5 G. Panneerselvam, V. Thirumal and H. M. Pandya, Review of Surface Acoustic Wave Sensors for the Detection and Identification of Toxic Environmental Gases/Vapours, *Arch. Acoust.*, 2018, **43**, 357–367.

6 U. Kumar, S. M. Huang, Z. Y. Deng, C. X. Yang, W. M. Haung and C. H. Wu, Comparative DFT dual gas adsorption model of ZnO and Ag/ZnO with experimental applications as gas detection at ppb level, *Nanotechnol*, 2022, **33**, 105502–105512.

7 C. Cheng, C. Chen, H. Zhang and Y. Zhang, Preparation and study of ammonia gas sensor based on ZnO/CuO heterojunction with high performance at room temperature, *Mater. Sci. Semicond. Process.*, 2022, **146**, 106700–106710.

8 P. Wu, Y. Li, S. Xiao, J. Chen, J. Tang, D. Chen and X. Zhang, SnO2 nanoparticles based highly sensitive gas sensor for detection of C4F7N: A new eco-friendly gas insulating medium, *J. Hazard. Mater.*, 2022, **422**, 126882.

9 K. S. Novoselov, D. Jiang, F. Schedin, T. J. Booth, V. V. Khotkevich, S. V. Morozov and A. K. Geim, Two-dimensional atomic crystals, *Proc. Natl. Acad. Sci. U. S. A.*, 2005, **102**, 10451–10453.

10 B. Wang, Y. Gu, L. Chen, L. Ji, H. Zhu and Q. Q. Sun, Gas sensing devices based on two-dimensional materials: a review, *Nanotechnol.*, 2022, **33**, 252001–252020.

11 C. Shen and S. Oyadiji, The processing and analysis of graphene and the strength enhancement effect of graphene-based filler materials: A review, *Mater. Today Phys.*, 2020, **15**, 100257–100283.

12 X. Gao, Y. Yao and X. Meng, Recent development on BN-based photocatalysis: A review, *Mater. Sci. Semicond. Process.*, 2020, **120**, 105256–105268.

13 R. Kumar, N. Goel, M. Hojamberdiev and M. Kumar, Transition metal dichalcogenides based flexible gas sensors, *Sens. Actuators, A*, 2020, **303**, 111875–111942.

14 P. Bhattacharyya and D. Acharyya, Impact of Device Configurations on Sensing Performance of WS_2 based Gas Sensors: A Review, *IEEE Sens. J.*, 2021, **21**, 22414–22425.

15 H. Mi, Q. Zhou and W. Zeng, A density functional theory study of the adsorption of Cl_2, NH_3, and NO_2 on Ag_3-doped WSe_2 monolayers, *Appl. Surf. Sci.*, 2021, **563**, 150329–1503237.

16 Y. Qiao, T. Hirtz, F. Wu, G. Deng, X. Li, Y. Zhi, H. Tian, Y. Yang and T. L. Ren, Fabricating molybdenum disulfide memristors, *ACS Appl. Electron. Mater.*, 2020, **2**, 346–370.

17 X. Zhang, Z. Lai, C. Tan and H. Zhang, Solution-processed two-dimensional MoS_2 nanosheets: preparation, hybridization, and applications, *Angew. Chem., Int. Ed.*, 2016, **55**, 8816–8838.

18 E. Lee and D. J. Kim, Recent exploration of two-dimensional MXenes for gas sensing:From a theoretical to an experimental view, *J. Electrochem. Soc.*, 2020, **167**, 037515–037527.

19 S. Sinha, Y. Takabayashi, H. Shinohara and R. Kitaur, Simple fabrication of air-stable black phosphorus heterostructures with large-area hBN sheets grown by chemical vapor deposition method, *2D Mater.*, 2016, **3**, 035010–035016.

20 M. S. Khan, A. Srivastava and R. Pandey, Electronic properties of a pristine and NH_3/NO_2 adsorbed buckled arsenene monolayer, *RSC Adv.*, 2016, **6**, 72634–72642.

21 J. Wu, Y. Wei, W. Shen, Y. Xiong, C. Lin, Y. Gao, A. AL-Ammari, K. Liu, T. Ma, J. Chen and H. Zeng, Antimonene nanosheets fabricated by laser irradiation technique with

outstanding nonlinear absorption responses, *Appl. Phys. Lett.*, 2020, **116**, 261903–261908.
22 K. Saito, M. Hasuo, T. Hatano and N. Nagasawa, Band gap energy and binding energies of Z_3-excitions in CuCl, *Solid State Commun.*, 1995, **94**, 33–35.
23 R. Girlanda, A. Quattropani and P. Schwendimann, Two-photon transitions to exciton states in semiconductors. Application to CuCl, *Phys. Rev. B: Condens. Matter Mater. Phys.*, 1981, **24**, 2009–2012.
24 D. C. Haueisen and H. Mahr, Resonant second-harmonic generation in the exciton region of CuCl and ZnO, *Phys. Rev. B: Solid State*, 1973, **8**, 734–735.
25 A. Zunger and M. L. Cohen, Electronic structure of CuCl, *Phys. Rev. B: Condens. Matter Mater. Phys.*, 1979, **20**, 1189–1192.
26 P. Hohenberg and K. J. Kohn, Density functional theory (DFT), *Phys. Rev.*, 1964, **136**, B864–B867.
27 P. Garg, K. S. Rawat, G. Bhattacharyya, S. Kumar and B. Pathak, Hexagonal CuCl monolayer for water splitting: a DFT study, *ACS Appl. Nano Mater.*, 2019, **2**, 4238–4246.
28 C. Xue, W. Hao, W. Cheng, J. Ma and R. Li, CO adsorption performance of CuCl/activated carbon by simultaneous reduction–dispersion of mixed Cu (II) salts, *Materials*, 2019, **12**, 1605–1609.
29 R. Zhang, H. Liu, B. Wang, J. Ren and Z. Li, Adsorption and dissociation of O_2 on CuCl (1 1 1) surface: A density functional theory study, *Appl. Surf. Sci.*, 2011, **258**, 408–413.
30 X. Sun, Q. Yang, R. Meng, C. Tan, Q. Liang, J. Jiang, H. Ye and X. Chen, Adsorption of gas molecules on graphene-like InN monolayer: A first-principle study, *Appl. Surf. Sci.*, 2017, **404**, 291–299.
31 L. Kou, T. Frauenheim and C. Chen, Phosphorene as a superior gas sensor: selective adsorption and distinct I–V response, *J. Phys. Chem. Lett.*, 2014, **5**, 2675–2681.
32 B. Zhu, K. Zheng, X. Chen, J. Qiu, H. Guo, F. Zhang, L. Lang, J. Yu and J. Bao, Monolayer Janus Te_2Se-based gas sensor to detect SO_2 and NO_x: a first-principles study, *Phys. Chem. Chem. Phys.*, 2021, **23**, 1675–1683.
33 Y. H. Zhang, Y. B. Chen, K. G. Zhou and Y. Peng, "Improving gas sensing properties of graphene by introducing dopants and defects: a first-principles study", *Nanotechnol.*, 2009, **20**, 185504–185509.
34 L. Chhana, B. Lalroliana, R. C. Tiwari, B. Chettri, L. Pachuau, S. Gurung, L. Vanchhawng, D. P. Rai, L. Zuala and R. Madaka, Theoretical Study of ZnS Monolayer Adsorption Behavior for CO and HF Gas Molecules, *ACS Omega*, 2022, **7**, 40176–40183.
35 B. A. Kalwar, W. Fangzong, A. M. Soomro, M. R. Naich, M. H. Saeed and I. Ahmed, Highly sensitive work function type room temperature gas sensor based on Ti doped hBN monolayer for sensing CO_2, CO, H_2S, HF and NO. A DFT study, *RSC Adv.*, 2022, **12**, 34185–34199.
36 N. Ahmadian, M. D. Ganji and M. Laffafchy, Theoretical investigation of nerve agent DMMP adsorption onto Stone–Wales defected single-walled carbon nanotube, *Mater. Chem. Phys.*, 2012, **135**, 569–574.
37 M. D. Ganji, S. Jameh-Bozorgi and M. Rezvani, A comparative study of structural and electronic properties of formaldehyde molecule on monolayer honeycomb structures based on vdW-DF prospective, *Appl. Surf. Sci.*, 2016, **384**, 175–181.
38 M. D. Ganji and M. Rezvani, Boron nitride nanotube based nanosensor for acetone adsorption: a DFT simulation, *J. Mol. Model.*, 2013, **19**, 1259–1265.
39 T. Banibairami, S. Jamehbozorgi, R. Ghiasi and M. Rezvani, Sensing behavior of hexagonal-aluminum nitride to phosgene molecule based on Van der Waals-density functional theory and molecular dynamic simulation, *Russ. J. Phys. Chem. A*, 2020, **94**, 581–589.
40 P. Giannozzi, S. Baroni, N. Bonini, M. Calandra, R. Car, C. Cavazzoni, D. Ceresoli, G. L. Chiarotti, M. Cococcioni, I. Dabo and A. Dal Corso, QUANTUM ESPRESSO: a modular and open-source software project for quantum simulations of materials, *J. Condens. Matter Phys.*, 2009, **21**, 395502–395520.
41 J. P. Perdew, K. Burke and M. Ernzerhof, Generalized gradient approximation made simple, *Phys. Rev. Lett.*, 1996, **77**, 3865–38668.
42 D. Vanderbilt, Soft self-consistent pseudopotentials in a generalized eigenvalue formalism, *Phys. Rev. B: Condens. Matter Mater. Phys.*, 1990, **41**, 7892–7894.
43 S. Grimme, Semiempirical GGA-type density functional constructed with a long-range dispersion correction, *J. Comput. Chem.*, 2006, **27**, 1787–1799.
44 H. J. Kulik, M. Cococcioni, D. A. Scherlis and N. Marzari, Density functional theory in transition-metal chemistry: A self-consistent Hubbard U approach, *Phys. Rev. Lett.*, 2006, **97**, 103001–103005.
45 S. L. Dudarev, G. A. Botton, S. Y. Savrasov, C. J. Humphreys and A. S. Sutton, Electron-energy-loss spectra and the structural stability of nickel oxide: An LSDA+U study, *Phys. Rev. B: Condens. Matter Mater. Phys.*, 1998, **57**, 1505–1509.
46 H. J. Kulik and N. Marzari, A self-consistent Hubbard U density functional theory approach to the addition-elimination reactions of hydrocarbons on bare FeO^+, *J. Chem. Phys.*, 2008, **129**, 134314.
47 J. R. Monteiro, C. Mota, M. S. Gusmao, A. Ghosh and H. O. Frota, Mechanical and dynamic stability of ZnX chalcogenide (X= O, S, Se, Te) monolayers and their electronic, optical, and thermoelectric properties, *J. Appl. Phys.*, 2021, **130**, 045110.
48 D. S. Lambert and D. D. O'Regan, Use of DFT+ U+ J with linear response parameters to predict non-magnetic oxide band gaps with hybrid-functional accuracy, *Phys. Rev. Res.*, 2023, **5**, 013160.
49 H. J. Monkhorst and J. D. Pack, Special points for Brillouin-zone integrations, *Phys. Rev. B: Solid State*, 1976, **13**, 5188–5192.
50 G. Henkelman, A. Arnaldsson and H. Jónsson, A fast and robust algorithm for Bader decomposition of charge density, *Comput. Mater. Sci.*, 2006, **36**, 354–360.
51 S. Peng, K. Cho, P. Qi and H. Dai, Ab initio study of CNT NO_2 gas sensor, *Chem. Phys. Lett.*, 2004, **387**, 271–276.

52 A. Allard and L. Wirtz, Graphene on metallic substrates: suppression of the Kohn anomalies in the phonon dispersion, *Nano Lett.*, 2010, **10**, 4335–4340.
53 B. V. Andryushechkin, K. N. Eltsov and V. M. Shevlyuga, CuI growth on copper surfaces under molecular iodine action: influence of the surface anisotropy in the iodine monolayer, *Surf. Sci.*, 2004, **566–568**, 203–209.
54 D. H. Fairbrother, J. G. Roberts, S. Rizzi and G. A. Somorjai, Structure of monolayer and multilayer magnesium chloride films grown on Pd (111), *Langmuir*, 1997, **13**, 2090–2096.
55 R. Hou, Y. Xia and S. Yang, A linear relationship between the charge transfer amount and level alignment in molecule/two-dimensional adsorption systems, *ACS Omega*, 2020, **5**, 26748–26754.
56 Z. Zhao, Y. Yong, Q. Zhou, Y. Kuang and X. Li, Gas-sensing properties of the SiC monolayer and bilayer: a density functional theory study, *ACS Omega*, 2020, **5**, 12364–12373.
57 T. Liu, Z. Cui, X. Li, H. Cui and Y. Liu, Al-doped $MoSe_2$ monolayer as a promising biosensor for exhaled breath analysis: a DFT study, *ACS Omega*, 2021, **6**, 988–995.
58 N. Barsan, D. Koziej and W. Weimar, Metal oxide-based gas sensor research: How to?, *Sens. Actuators, B*, 2007, **121**, 18–35.